Korean J. Chem. Eng., 39(3), 646-654 (2022)
DOI: 10.1007/s11814-021-0958-2

pISSN: 0256-1115
eISSN: 1975-7220

17α-Ethinylestradiol elimination using synthesized and dense nanocomposite materials: Mechanism and real matrix treatment

Ralte Malsawmdawngzela and Diwakar Tiwari†

Department of Chemistry, Mizoram University, Aizawl-796004, India
(*Received 14 July 2021 • Revised 12 September 2021 • Accepted 14 September 2021*)

Abstract−Endocrine disrupting chemicals (EDCs) are emerging water contaminants and efficient elimination is a greater challenge for environmental engineers. The present communication is intended to synthesize the novel dense nanocomposite materials precursors to the bentonite and 3-mercaptopropyletrimethoxy silane/or 3-aminopropyl-etriethoxy silane. The materials are highly dense, hence the surface area is significantly reduced compared to the pristine bentonite. Further, the materials are intended to be utilized in the elimination of one of the important EDC 17α-ethinylestradiol (EE2). The sorption mechanism is greatly demonstrated based on various parametric studies. It is shown that grafted silane with bentonite network provides enhanced hydrophobicity with organophilic nature and greatly favors the uptake of EE2 at a wide range of pH (5.0-10.0). Relatively rapid uptake of EE2 by the nanocomposite solids followed by a pseudo-second-order kinetic model indicated that the materials are highly efficient for elimination of EE2. Increasing the concentration of EE2 (1.0 to 10.0 mgL^{-1}) favored the extent of removal of EE2 and followed the Langmuir adsorption isotherm. Further, the increase in background electrolytes by 1,000 times did not affect the removal of EE2 by these nanocomposites, indicating the sorbing species are attracted with relatively stronger forces. Moreover, the simultaneous presence of several co-ions did not affect the percentage elimination of EE2; this, perhaps, shows an enhanced selectivity of materials towards the 17α-ethinylestradiol. A high loading capacity of EE2 is achieved under column reactor operation using these nanocomposites. Additionally, the materials are promising in the real matrix treatment.

Keywords: 17α-Ethinylestradiol Elimination, Real Matrix Treatment, Nanocomposites, Silane Grafted Bentonite, Fixed-bed Treatment, Hydrophobic Interactions

INTRODUCTION

An enhanced level of emerging micro-pollutants, including pharmaceuticals or personal care products, in water bodies has received global attention and it poses greater challenges to maintaining water quality. The diverse chemical compositions and potential of micro-pollutants, as well as the intricate network of exposure pathways, create innumerable problems to researchers or regulatory bodies for possible solutions [1,2]. These pollutants are increasingly entering into the terrestrial environment as toxic chemicals, and due to their persistence in nature are partly eliminated from biological treatment plants. It is pointed out that even at low concentrations, these micro-pollutants are active and stable in the water bodies, which shows a long exposure to aquatic life [3]. Similarly, the endocrine disrupting chemicals (EDC) are posing serious concern due to the negative impact on human beings [4]. The Environmental Protection Agency (EPA) has described endocrine disruptors (EDC's) as, "exogenous compounds which intervene the production, emission, binding and movement of natural hormones which are essential for the growth and function of living organisms" [5]. EDC's are classified as natural and synthetic estrogens, which affect the biological systems of aquatic organisms even at very low concentrations, i.e., 0.1 ngL^{-1} [6]. The most harmful endocrine disruptor is known to be ethinyl estradiol (EE2), the major primary substance used in contraceptive pills and postmenopausal hormone supplements [4,7,8]. EE2 is commonly detected in domestic sewage systems and some industrial wastewaters [9,10]. Human urine is regarded as the primary source of estrogens in wastewater [11]. Previous study reported that a significant amount of free EE2 is detected in wastewaters and having the concentration of 7-42 ngL^{-1} from the effluents of wastewater treatment plants [12]. It was also reported that treated water for drinking in Germany contained a significant amount of EE2 at 0.5 ngL^{-1} [13]. According to several reports, human health is significantly affected by EE2 and causes diseases such as disorders of the reproductive system, cancer and impotence [14-16]. Compared to natural estrogens, the half-life of EE2 is longer and is more harmful [17]. EE2 is readily gathered in silt and ecosystems [18] and hence, the concentrations of EE2 ranged from 0.1-10 ngL^{-1} which affected the life of fish and other organisms in water [19]. Research conducted by spiking a lake in Canada with EE2 concentration 5-6 ngL^{-1}, resulted in the deaths of the entire fish population [20].

Several methods, including adsorption [21], advanced oxidation process [22], membrane filtration [23], biological treatment [24] are often demonstrated for efficient removal of EE2. Among these methods, adsorption using advanced and efficient materials has attracted greater interest in elimination or retaining contaminants [25,26]. The method is versatile and sorption properties can

†To whom correspondence should be addressed.
E-mail: diw_tiwari@yahoo.com

be regulated with suitable modification or even functionalization of materials. Additionally, the porosity of materials further plays an important role in designing the treatment process for specific pollutants [27-30].

Sorption of EE2 and BPA on mesoporous material, anthracite was conducted using site energy distribution (SED) analysis. Results showed that EE2/or BPA is first aggregated on high-energy sites followed by lower energy sorption sites on the anthracite. Further, at neutral pH, it is evidenced that hydrogen bonding and π-π electron donor-acceptor (EDA) interaction is predominant for BPA adsorption whereas the EE2 was sorbed with the ligand-exchange process in addition to the hydrogen bonding and EDA [31]. Similarly, sorption of EE2 on M9CTA$^+$, M16CTA$^+$ and M34CTA$^+$ composite materials has the sorption capacity of 4.3, 8.8 and 7.3 mgg^{-1}, respectively. It is indicated that the hydrophobic cavity is providing space for sorption of EE2 [32].

A hybrid method based on the photocatalytic with sonolysis was employed for the removal of potential micropollutant: lovastatin from aqueous solutions [33]. Similarly, the sono-photo-ferrioxalate system was introduced in the degradation of recalcitrant pollutants producing less by-products. [34]. The adsorption and degradation of pharmaceuticals using metal-free polymeric catalyst, graphitic carbon nitride (g-C_3N_4) showed that degradation is primarily due to the oxidation process. Degradation is more effective under UV-C than UV-A light irradiation due to the reactive species ($^{\bullet}$OH, $^{\bullet}$H, $^{\bullet}$O, $O_2^{\bullet-}$, $HO_2^{\bullet}$ etc.) formed through ionization and excitation of water molecules. [35]. A series of g-C_3N_4 photocatalysts was prepared using hydrothermal method and employed for the degradation of EE2. The result showed that kinetic constant of EE2 degradation using g-C_3N_4-3 (alkaline-modified) was nearly 3.5-fold that of g-C_3N_4-1 (pure). Further, hydrothermal treatment result showed a decrease in the recombination rate of photogenerated e^-/h^+ pairs. The degradation of EE2 in buffered water and in HWW is governed by photoreduction by superoxide radicals, which is the main mechanism for the degradation of EE2 in buffered water and hospital wastewater. The elimination of estrogenicity in the photocatalytic treated samples was confirmed by YES assay [36]. It was also reported that EE2 was effectively degraded through a combination of photocatalysis using peroxide/low-pressure ultraviolet (UV) treatment followed by biological treatment using small bioreactor platform capsules [37]. Polyacrylonitrile (PAN) beads are utilized in the elimination of EE2 in aqueous solution. Adsorption isotherm is fitted well to Freundlich adsorption isotherm. Further, the kinetic data reveals that the sorption process proceeded through chemisorption [38]. Sorption of EE2 on aliphatic polyamides (PA612) shows that hydrogen bonding occurred between the EE2 and PA612 in the adsorption process [39]. Similarly, sorption of EE2 on activated charcoal was mainly governed by the film diffusion process and the maximum sorption capacity was obtained at neutral pH [40]. It was also reported that the removal of 17α-ethynylestradiol (EE2) from water using three upstream bioreactors (UBRs), filled with granulated activated carbon (GAC), sand, or MnO_2 granules was 99.8%, 17.3% and 81.7%, respectively. The EE2 was primarily adsorbed by the GAC and MnO_2 showing synergistic in the removal of EE2 in reactor operations [41]. Ionic liquid cholinium alaninate (N_{1112O}HAla) was employed to separate 17-β estradiol and tetracycline and fluoroquinolone families in the aqueous synthetic swine effluent. Results showed that the most hydrophobic contaminant (E2) was favorably partitioned to the surfactant rich phase, independent of the feed composition. Conversely, the initial concentration of the salting out agent strongly affected the removal of antibiotics, and the incorporation of CTAB allowed to enhance the removal values at levels greater than 90% [42].

Clay minerals are ubiquitous in nature and show widespread applications in the decontamination of water contained with a variety of pollutants, including heavy metal toxic ions [43-46]. Although clay samples are efficient in the removal of heavy metal toxic ions, however, possessing limited applicability towards the oxyanions or the micro-pollutants in aqueous media [47,48]. Therefore, the present investigation intended to functionalize the bentonite using the organosilane (3-mercaptopropyletrimethoxy and 3-aminopropyletriethoxy silane) by sol gel process. This enables one to obtain a dense nanocomposite solid which is likely to efficiently remove the EE2 in aqueous wastes. The mechanistic aspects in the sorption process along with real matrix treatment were extensively conducted for possible implication of novel materials in the waste treatment.

MATERIALS AND METHODS

1. Materials

Bentonite was collected from Gujarat, India. It was washed with distilled water dried at 100 °C and sieved with 100 BS (British Standard) Sieve to obtain the 0.150 mm particles. 3-mercaptopropyletrimethoxy silane, 3-aminopropyletriethoxy silane and 17α-ethynylestradiol (EE2) are of Sigma, Aldrich, USA products. Ethylenediaminetetraacetic acid was procured from Qualigens India Ltd., India. Magnesium sulfate heptahydrate was of Loba Chemie, India, product. Calcium chloride dihydrate powder, manganese (II) chloride, oxalic acid, di-sodium hydrogen phosphate anhydrous purified, aluminium (III) chloride and nickel chloride were procured from Merck, India. Sodium chloride (Extrapure) and glycine were obtained from HiMedia, India.

2. Methodology

2-1. Synthesis of Silane Functionalized Bentonite

Silanes were grafted with bentonite clay using a simple one pot synthetic route. Dried bentonite (BN) (15 g) was introduced in 300 mM of toluene. Further, under stirring the suspension was refluxed for 30 min at 70 °C under nitrogen atmosphere. 3-mercaptopropyletrimethoxy silane (15 mL) was introduced dropwise to the suspension and further refluxed for 24 hrs. The suspension was filtered and washed with toluene and ethanol. The sample was dried at 90 °C overnight. The dried nanocomposite was stored in a polyethylene bottle and named as MPTS@BN. A similar procedure was employed for the grafting 3-aminopropyletriethoxy silane with bentonite, and the nanocomposite material was assigned as APTES@BN. The point of zero charge (pH_{PZC}) of the pristine bentonite and the two nanocomposite materials were obtained using the acid base titration method as demonstrated previously [49].

2-2. Characterization and Surface Morphology of Materials

The functional groups present in bentonite (BN), MPTS@BN and APTES@BN were obtained by using FT-IR (IR Affinity Shimadzu, Japan) analysis. Surface morphologies of bentonite, MPTS@BN and

APTES@BN were obtained by field emission scanning electron microscope (FE-SEM; S-4700, Hitachi, Japan) and the elemental mapping of solids was carried out using the energy-dispersive X-ray spectroscopy (EDX) as coupled with the SEM machine. The structural property of the materials was evaluated by the X-ray diffraction method (Philips X'pert MPD System). Further, the specific surface area, pore size and pore volume of the materials were acquired by using BET Analyzer (Micromeritics, ASAP 2010, France).

2-3. Batch Reactor Studies

EE2 stocks solution (25.0 mgL^{-1}) was prepared and diluted to required experimental concentrations by successive dilution. Various physico-chemical parametric experiments (pH study, contact time, presence of co-existing ions, presence of background electrolyte concentrations, sorptive concentrations) were conducted in the batch reactor studies. 50.0 mL of EE2 solution was taken into different polyethylene bottles and 100 mg of the nanocomposite solid was added to these solutions. These bottles were closed tightly and shaken for 24 hrs at 25 °C in an automatic shaker (Incubator-Shaker, TM Weiber, ACMAS Technologies Pvt. Ltd., India). These samples were then filtered with a 0.45 µm syringe filter and the pH was measured again and reported as final pH. The filtrates along with the blank samples were analyzed with UV-Vis spectrophotometer (Shimadzu Model: UV 1800, Japan) at 280 nm for EE2. Different concentrations of EE2 solutions, 1.0, 3.0, 5.0, 7.0 and 10.0 mgL^{-1}, were used to obtain the calibration curve for EE2 at 280 nm. The concentration of EE2 was varied from 1.0 to 10.0 mgL^{-1} at pH 4.0 to analyze the effect of sorptive concentrations in the elimination of EE2 by nanocomposite solids. The time dependence elimination of EE2 by nanocomposite solids was performed at definite time intervals using initial concentration of EE2 10.0 mgL^{-1} at pH 4.0 and 25 °C. The results are presented as percentage elimination of EE2 at different times of contact. Background electrolyte concentrations studies on the removal of EE2 were conducted by increasing the concentration of NaCl from 0.0001 to 0.1 $molL^{-1}$ having EE2 concentration of 10.0 mgL^{-1} and at constant pH of 4.0 and at 25 °C. The sorption of EE2 in presence of several co-ions, such as anions (ethylenediaminetetraacetic acid, glycine, oxalic acid and phosphate) and cations (Mg(II), Mn(II), Ni(II), Ca(II)) was studied using the nanocomposite materials. The concentration of EE2 was taken as 10.0 mgL^{-1} at constant pH 4.0 and co-ion concentration of 50.0 mgL^{-1} at 25 °C. Results are demonstrated as percent elimination of EE2 in the presence of several co-ions.

2-4. Fixed Bed Column Studies

The sorption of EE2 by nanocomposite solids was performed under fixed-bed column experiments using a glass column (10 mm diameter). The nanocomposite material 0.25 g/or 0.5 g was taken in the column along with sand particles (2.5 g). The nanocomposite was placed in the middle of the column and above and below to nanocomposite solid sand was placed. Remaining column was packed with the glass beads. Solution of EE2 (10.0 mgL^{-1}, pH 4.0) was pumped upward from the bottom of the column using a peristaltic pump at a constant flow rate of 1.0 $mLmin^{-1}$ and effluent samples were collected using a fraction collector. The effluent solution was filtered and filtrates were analyzed using UV-vis spectrophotometer. The loading capacity of the nanocomposite materials under continuous flow system was obtained using the Thomas equation [50].

RESULTS AND DISCUSSION

1. Characterization of the Material

The FT-IR spectra of BN, MPTS@BN and APTES@BN materials showed weak peaks at 2,927 cm^{-1} and 2,858 cm^{-1} due to the stretching vibration of -CH_3 and -CH_2, respectively [51] (*Cf* Fig. 1(a)). A distinct peak at 2,927 cm^{-1} is due to the methoxy group (-OCH_3) present with MPTS@BN [52,53]. The stretching vibration of -SH group from MPTS is observed at 2,550 cm^{-1} (weak vibrations) [54]. Two peaks at 682 and 1,402 cm^{-1} are due to the deformation vibrations of C-H and stretching of thiol group from MPTS, respectively [55]. Similarly, APTES@BN shows the aliphatic CH_2 bending vibrations as a weak peak is observed at 1,485 cm^{-1} [56]. The stretching vibration bond of C-N occurs by a subtle peak at ~1,319 cm^{-1}, which further confirms the presence of organosilane grafted with the bentonite network [57]. The symmetric stretching vibrations of the methylene group from the organosilane also occurred by a small but distinct peak at 2,894 cm^{-1} [58].

The Brunauer, Emmett, and Teller (BET) method was utilized to obtain the specific surface area, pore volume, and pore size of BN, and MPTS@BN and APTES@BN solids. Fig. 1(b) shows the nitrogen adsorption-desorption isotherms for these two nanocomposite materials. It is evident from the figure that the pristine bentonite, MPTS@BN and APTES@BN showed type IV isotherms with H3 type hysteresis loop. This implied that the solid samples contained predominantly a mesoporous structure [59,60]. Further, it is noted that the pristine bentonite is having a broader hysteresis loop with the pore size of 68.43 Å and pore volume of 0.077 cm^3g^{-1}.

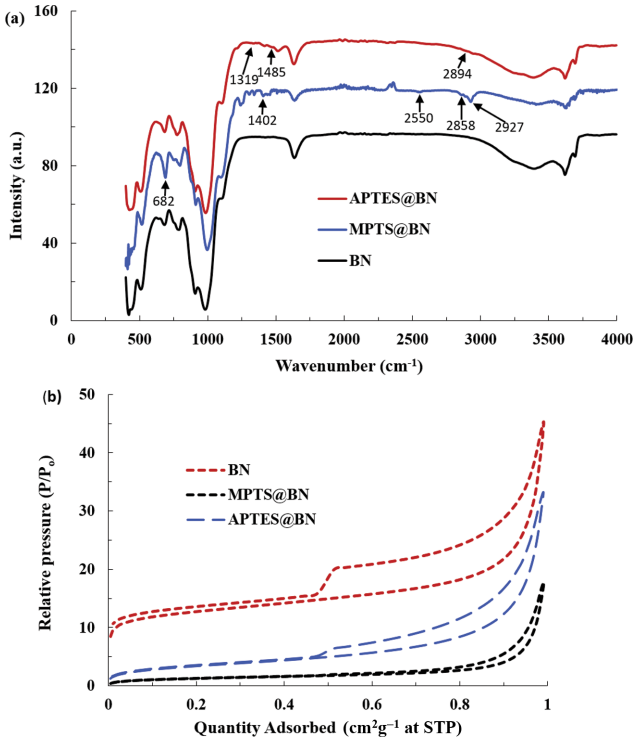

Fig. 1. (a) FT-IR spectra; and (b) nitrogen adsorption-desorption isotherms obtained for pristine bentonite (BN) and MPTS@BN and APTS@BN nanocomposites.

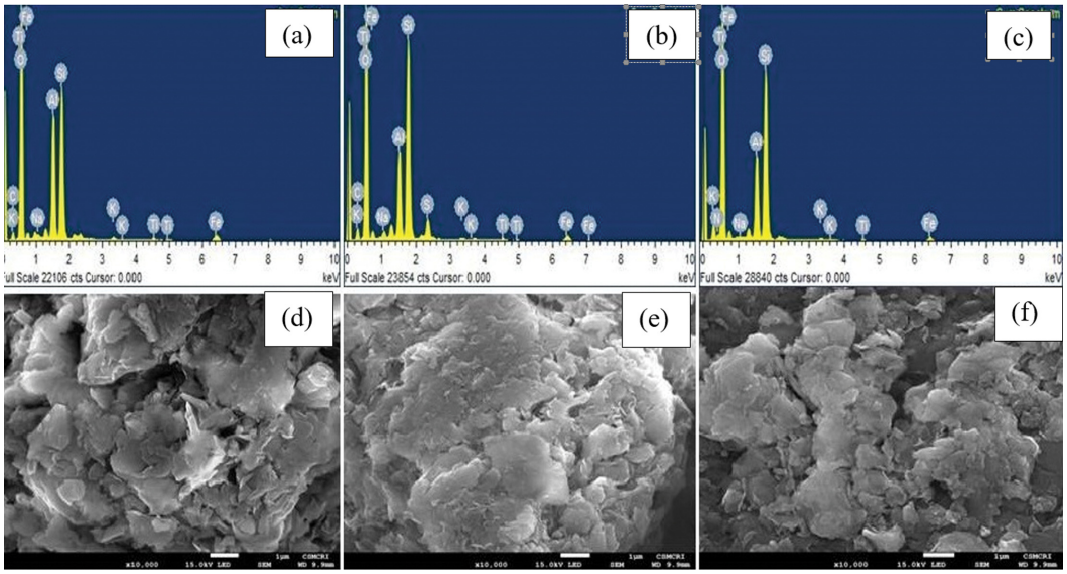

Fig. 2. EDX analytical graph of (a) pristine bentonite; (b) MPTS@BN; (c) APTES@BN and SEM image of (d) pristine bentonite; (e) MPTS@BN; and (f) APTES@BN.

The pore size and pore volume of MPTS@BN and APTES@BN are found to be 68.39 Å, 0.070 cm^3g^{-1} and 165.13 Å, 0.051 cm^3g^{-1}, respectively. The BET specific surface area of BN, MPTS@BN and APTES@BN was found to be 41.11, 4.68 and 12.52 m^2g^{-1}, respectively. The specific surface areas of both the nanocomposite materials exhibit a significant decrease in surface area once organosilane is grafted with the bentonite network. This decrease in specific surface area is because the organo-silanes MPTS/APTES occupy the pores of the bentonite layers and, hence, decreased the specific surface area of solids. Previously, it was reported that grafting of MPS and APS onto silica gels significantly decreased the surface area of the materials [61]. Grafting of attapulgite with (3-aminopropyltriethoxysilane) also exhibited a substantial decrease in the specific surface area of the material [62].

The SEM images of BN, MPTS@BN and APTES@BN are shown in Fig. 2. Morphological images of these solids showed that these solids possessed heterogeneous and disordered surface structure. Pristine bentonite exhibits fairly good porosity, which is significantly reduced with the solids MPTS@BN or APTES@BN. This is due to the grafting of MPTS/or APTES molecules within the pores of bentonite. The materials are denser and more compact but possessed with high hydrophobic and organophilic nature. Natural attapulgite had a loose aggregate structure but after grafting with (3-aminopropyltriethoxysilane) the modified material had a compact aggregate structure [63]. These results are consistent with the textural properties obtained by the BET analyses. Moreover, the elemental mapping of BN, MPTS@BN and APTES@BN was obtained using energy-dispersive X-ray spectroscopy (EDX) and results are shown in Fig. 2((a), (b) & (c)). The figure clearly implies that the sulfur and nitrogen peaks are observed in the EDX spectra of MPTS@BN and APTES@BN, respectively. The sulfur and nitrogen peaks are not observed in the pristine bentonite. The presence of nitrogen (N) and mercapto (-SH) confirmed the grafting of organosilanes with bentonite. These results further entailed the successful grafting of MPTS/or APTES molecules within the bentonite network. It was reported previously that the silicon (Si) and sulfur (S) peaks are observed in the EDX mapping on mercaptopropyl-coated SiO_2 particles [64]. Modification of bentonite with 3-aminopropyletrimethoxysilane showed the predominant peaks of N and C in the EDX analysis [65]. Results obtained using CHN elemental analysis in the modification of mesoporous SBA-15 with amino-propyl silane showed the presence of nitrogen along with enhanced carbon percentage [66].

2. Effect of pH on the Removal of EE2

The pH dependence sorption of EE2 is shown in Fig. 3. It is evident from the figure that the elimination of EE2 by the BN is quite low within the studied pH (pH 3.0-10.2). A maximum of *Ca* 43% was recorded at pH 5.8. However, using the nanocomposite solids (MPTS@BN and APTES@BN) showed significantly enhanced elimination of EE2 within the studied pH (3.0-10.2). It is further noted that a maximum of *Ca* 85% and and 74% of EE2 is elimi-

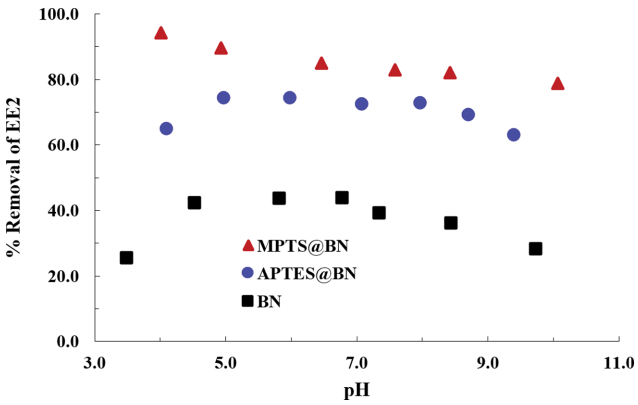

Fig. 3. pH dependence sorption of EE2 by BN, MPTS@BN and APTES@BN solids.

nated using the MPTS@BN and APTS@BN solids at around pH 6.0. The acid dissociation constant (pk_a) of EE2 is reported as 10.5 [67]. Therefore, the EE2 exists as neutral species pH<<10.5 and carries net negative charge pH>>10.5. On the other hand, the pH_{pzc} (point of zero charge) of BN, MPTS@BN and APTES@BN is obtained as 7.79, 7.72 and 7.64, respectively. Therefore, a high removal of EE2 by using the nanocomposite solids at a wide range of pH is demonstrated with the hydrophobic interaction between the EE2 and MPTS@BN and APTES@BN solids. The organo-silanes introduced within the bentonite sheets provide enhanced hydrophobicity with the organophilic nature which is intended to attract the EE2 molecules and enable a high uptake of EE2. Moreover, the dense grafted structure of MPTS@BN and APTES@BN has enabled to significantly trap the EE2 from aqueous solutions and enhance the elimination of EE2. Further, it is noted that the removal of EE2 by the MPTS@BN showed very high uptake, which was almost unaffected within the pH region pH 4.0-10.0. This indicates that the EE2 showed very high affinity towards the denser composite solid (having specific surface area of 4.68 m^2g^{-1}) and hence, the dense material traps efficiently the EE2. Similar results were reported for the removal of As(V) using the MPTS grafted chitosan where it was assumed that the introduced silanes provide sorbing sites along with the siloxane sites. Hence, the As(V) forms weaker bonds, enhancing the percentage removal [68]. On the other hand, the APTS@BN showed slightly less adsorption at lower pH value, i.e., pH~4.0. However, almost a constant removal of EE2 was obtained within the pH region: pH~5.0-9.0. The low removal at pH 4.0 is possibly due to the competition between the H^+ and EE2 towards the solid surface. Additionally, it is observed that APTS@BN showed relatively less percentage removal compared to the MPTS@BN. This is because the APTS@BN is relatively less dense material compared to the MPTS@BN since the specific surface area of APTS@BN is relatively , i.e., 12.52 m^2g^{-1}. This restricted partly the uptake of EE2 by APTS@BN. A similar result in the removal of EE2 is reported using activated carbon powder [69] or even As(V) by APTS grafted chitosan [70]. Moreover, compared to two nanocomposite solids, MPTS@BN and APTS@BN, the MPTS@BN showed relatively higher percentage removal of EE2 throughout the studied pH (3.0-10.0). This indicates the higher affinity of materials for EE2.

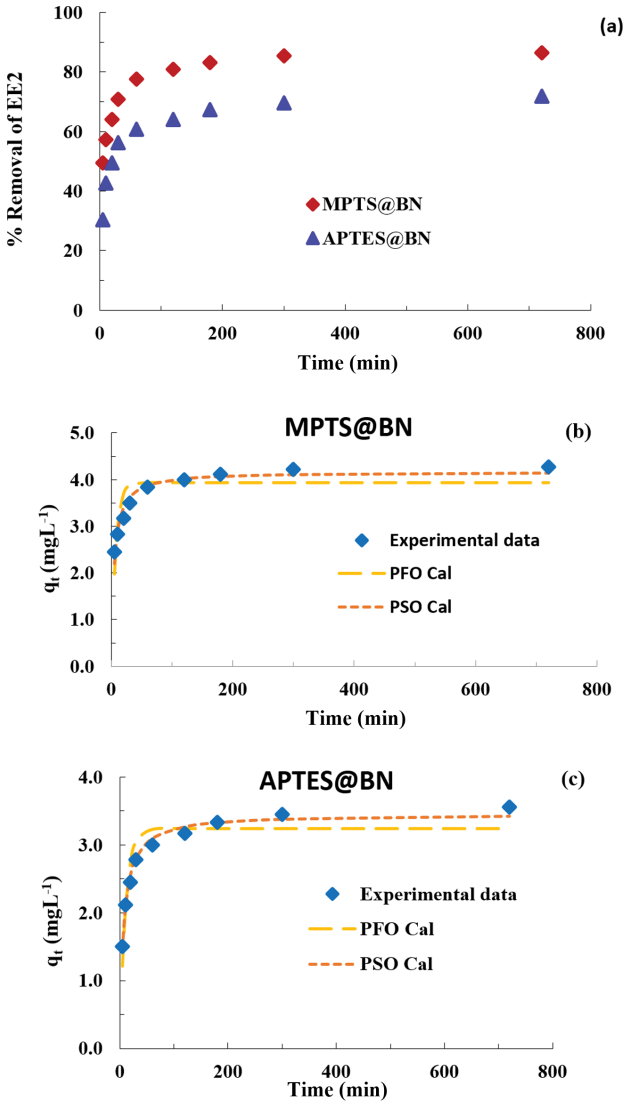

Fig. 4. (a) Effect of contact time in the elimination of EE2 by MPTS@BN and APTES@BN nanocomposites (pH: 4.0; [EE2]: 10.0 mgL^{-1}; dose: 2.0 gL^{-1}). Plots of PFO and PSO kinetic models for the sorption of EE2 by (b) MPTS@BN; and (c) APTES@BN nanocomposites.

3. Time Dependence Sorption of EE2

Sorption efficiency of EE2 by MPTS@BN/ or APTES@BN *vs* time was obtained and shown in Fig. 4(a). The percent removal of EE2 by both the nanocomposite materials is rapid during the initial period of contact and *Ca* 57% and *Ca* 42% of EE2 is removed within 10 min of time by the MPTS@BN and APTES@BN materials, respectively. Further, the sorption of EE2 onto these nanocomposites saturates just within 120 min. This indicates that the surface active sites of these two nanocomposite materials saturates within 120 min and no further removal of EE2 is observed even after 720 min of contact [71]. These results further implied that both the nanocomposite materials possessed high affinity for the attenuation of EE2 and its applicability in treatment of wastewater.

The adsorption kinetics of EE2 using MPTS@BN and APTES@BN employing pseudo-first order (PFO) and pseudo-second order

Table 1. Estimated kinetic constants for pseudo-first order and pseudo-second order uptake of EE2 by solid materials

Pollutant	Materials	PFO Model			PSO Model		
		q_e (mgg^{-1})	k_1 (min^{-1})	s^2	q_e (mgg^{-1})	k_2 ($M^{-1}min^{-1}$)	s^2
EE2	MPTS@BN	3.94	0.139	0.898	4.172	0.053	0.171
	APTES@BN	3.24	0.093	0.47	3.457	0.041	0.064

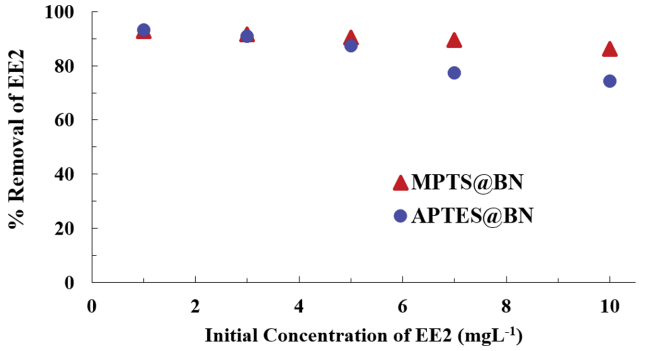

Fig. 5. Percentage removal EE2 at different initial concentrations of EE2 using APTES@BN and MPTS@BN nanocomposites.

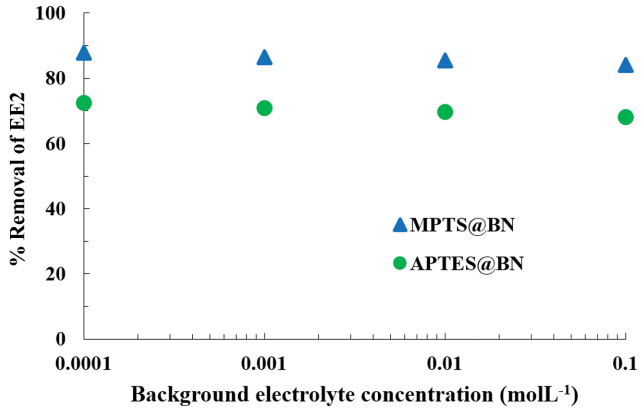

Fig. 6. Effect of background electrolyte concentrations in the elimination of EE2 by nanocomposite MPTS@BN and APTES@BN materials.

(PSO) kinetic models [70] and the non-linear simulation results are presented in Fig. 4((b) and (c)). Further, the optimized results are shown in Table 1. The results show that PSO model is fitted well since the least square sum is significantly low compared to PFO. The sorption of EDCs (trimethoprim (TMP), estrone (E1), 17β-estradiol (E2) and 17α-ethynilestradiol (EE2)) using SnO_2 pillared montmorillonite also followed PSO kinetic model [72]. Further, it is observed that MPTS@BN and APTES@BN materials possessed high elimination capacity for EE2. This affirms the greater applicability of nanocomposites in the remediation of aqueous waste contaminated with EE2.

4. Concentration Dependent Study

The relationship between the initial EE2 concentration (1.0, 3.0, 5.0, 7.0 and 10.0 mgL^{-1}) and percent removal of EE2 by the MPTS@BN and APTES@BN materials was obtained at pH 4.0 having nanocomposite dose 2.0 gL^{-1} at 25 °C. The results are illustrated in Fig. 5. Results indicate that by increasing the concentration of EE2, the percentage elimination of EE2 is decreased significantly. Increasing concentration of EE2 from 1.0 to 10.0 mgL^{-1}, the decrease in percent elimination of EE2 is from 93.3 to 74.4% for APTES@BN and from 92.8% to 86.1% for APTES@BN. A very high percent uptake of EE2 even at high concentration of EE2 implied the high affinity of MPTS@BN and APTES@BN materials for EE2.

The linear form of Langmuir and Freundlich isotherms was utilized for isotherm modelling of EE2 towards the MPTS@BN and APTES@BN [73] and results are illustrated in Fig. S1((a) and (b)) (Supplementary materials). The unknown constants are estimated and presented in Table 2. This showed that the Langmuir isotherm was better fitted compared to the Freundlich isotherm. A high value of Langmuir monolayer capacity was achieved for EE2 using both the materials. The sorption of 17β-estradiol, 17α-ethinylestradiol and bisphenol A on tea leaves (TL_H) also followed the Langmuir adsorption isotherm model [74].

5. Effect of Background Electrolyte Concentrations

The impact of background electrolyte (NaCl) (0.0001, 0.001, 0.01 and 0.1 $molL^{-1}$) concentrations on the adsorption of EE2 by nanocomposite materials was studied as this enables to deduce the type of interactions involved between the sorbate species and sorbent. Elimination of EE2 using the MPTS@BN and APTES@BN materials is unaffected by increasing the background electrolyte concentrations of NaCl for 1,000 times (*Cf* Fig. 6). These results imply that a 1,000 times increase in background electrolyte concentration has not affected the percent sorption of EE2 by the nanocomposites. This confirms that sorbate species EE2 enters into the Stern layer at the surface and bonds with relatively stronger forces. This indicates that the EE2 is interacting at the surface of nanocomposite solids with hydrophobic interactions and proceeding with organophilic attractions. Earlier, it was mentioned that the presence of background electrolyte (NaCl) has not affected the percentage elimination of EE2 by advanced materials [75]. Increasing ionic strength of NaCl from 0-320 mM in leachate solutions has not affected sorption of bisphenol A and EE2 by SWCNTs [76]. Sorption of estrone (E1), 17β-estradiol (E2) and 17α-ethinyl estradiol (EE2) using n-propyl functionalized mesoporous material (30% Pr-MCM-41) on increasing the concentration of NaCl from 0.001-0.1 $molL^{-1}$ did not significantly affect the elimination of E1, E2 and EE2. This result is due to the same contribution produced by salting effect for estrogens and squeezing-out effect for 30%Pr-MCM-41 in presence of co-existing ions. The high removal of estrogens is due to the π-π and hydrophobic interactions between

Table 2. Langmuir and Freundlich isotherm constants along with the R^2 values obtained for the sorption of EE2 by nanocomposite MPTS@BN and APTES@BN materials

Materials	Langmuir			Freundlich		
	q_o (mgg^{-1})	b (Lg^{-1})	R^2	1/n	K_f (mgg^{-1})	R^2
MPTS@BN	8.1	0.888	0.999	0.577	5.277	0.988
APTES@BN	4.283	1.774	0.972	0.392	2.935	0.959

Table 3. Thomas constants estimated in the removal of EE2 using nanocomposite MPTS@BN and APTES@BN materials

Nanocomposite materials	Weight of nanocomposite materials (g)	Thomas constants		Least square sum (s^2)
		q_o (mgg^{-1})	K_T ($Lmin^{-1}mg^{-1}$)	
MPTS@BN	0.25	17.07	8.32×10^{-4}	3.1×10^{-2}
	0.50	20.75	6.27×10^{-4}	5.1×10^{-3}
APTES@BN	0.25	11.23	1.23×10^{-3}	1.1×10^{-2}
	0.50	16.57	7.03×10^{-4}	3.8×10^{-3}

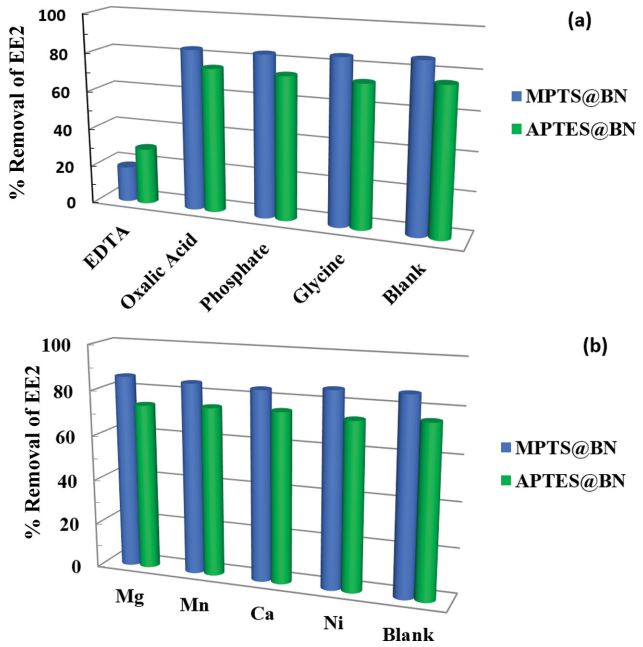

Fig. 7. Percent removal of EE2 by nanocomposite materials in presence of (a) anions; and (b) cations.

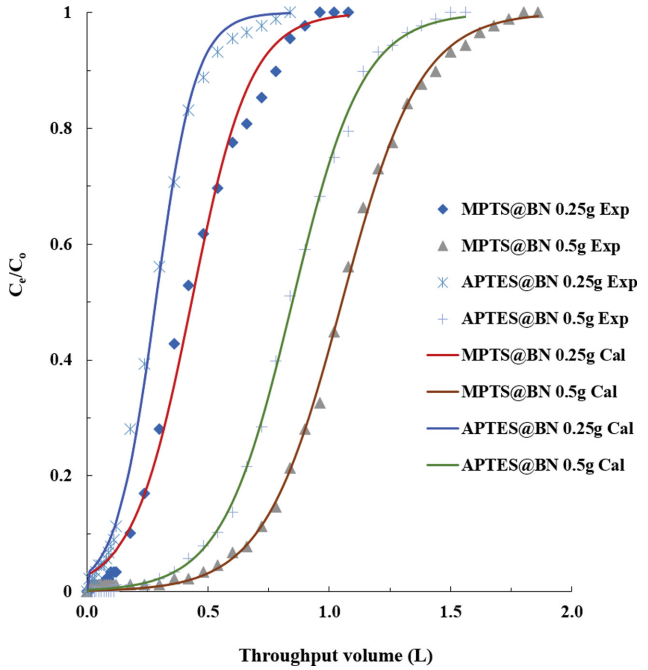

Fig. 8. Breakthrough curves obtained for the removal of EE2 using composite (MPTS@BN and APTES@BN) material [Influent concentration of EE2: 10.0 mgL^{-1} (pH 4.0); Flow rate: 1.0 mL min^{-1}].

the 30%Pr-MCM-41 and estrogens [77].

6. Co-ions Effect

Co-ions (cations: Mg, Mn, Ca and Ni or anions: oxalic acid, glycine and phosphate) may affect the elimination of EE2 by MPTS@BN and APTES@BN materials. The concentration of EE2 and co-ions was taken as 10.0 mgL^{-1} and 50.0 mgL^{-1}, respectively, at pH 4.0. Results are shown as percentage elimination of EE2 in presence of these co-existing ions (*Cf* Fig. 7). The percentage removal of EE2 was not changed in the presence of these co-ions, except EDTA, which significantly affected the removal of EE2 by these two nanocomposite solids. This is possibly due to the competitive sorption of EDTA towards solid surface. It was previously reported that the sorption of EE2 using PA612 was unaffected in the presence of cations (0.1 $molL^{-1}$) such as Zn(II), K(I) or Ca(II); however, only a slight reduction in sorption was monitored in the presence of Mg (II) [8].

7. Column Studies for EE2

The loading capacity of nanocomposite MPTS@BN and APTES@BN materials was determined using column experiments under dynamic conditions. Fig. 8 shows the breakthrough curves of EE2 using MPTS@BN and APTES@BN packed columns. The nanocomposite solids had relatively high breakthrough volumes for EE2. Further, it was observed that increasing the amount of nanocomposite solids in the column enabled to increase the breakthrough volume of EE2. A complete breakthrough for EE2 was achieved having throughput volume of 0.84 L and 1.50 L using 0.25 g and 0.5 g APTES@BN, respectively. Similarly, a complete breakthrough was attained at the volume of 0.96 L and 1.80 L using 0.25 g and 0.5 g of MPTS@BN, respectively. Breakthrough data is intended to utilize a non-linear least square fitting using Thomas equation. The fitting results are illustrated in Fig. 8. Moreover, optimized constants are returned in Table 3. Results show that under the dynamic conditions, the MPTS@BN and APTES@BN possessed high loading capacity for EE2. This again reaffirmed that the novel nanocomposite solids have potential in the elimination of EE2 from aqueous wastes.

8. Removal of EE2 in Real Water Sample

The removal of EE2 using real matrix samples was conducted under different pH values. The water sample was collected from Kawnpui river at Kolasib District, Mizoram, India. The physicochemical analysis of river water is presented in Table S1 (Supplementary Materials). The pH of river water was found to be 7.23.

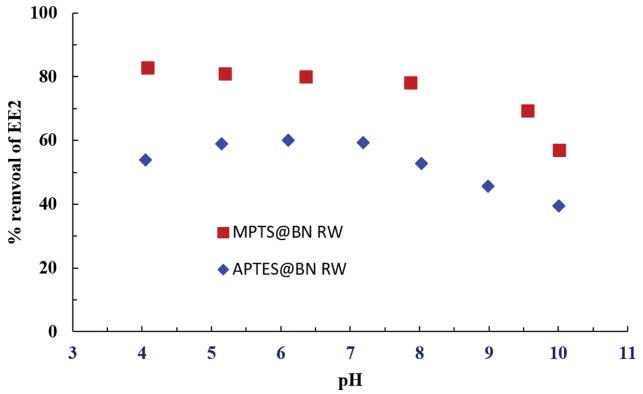

Fig. 9. Effect of pH in the sorption of EE2 by nanocomposite materials in real water sample.

The sample contained low levels of Fe, Mn, Ca, and Zn. However, relatively high levels of Ca were present. The river water had high level of non-purgeable organic carbon (NPOC) along with some inorganic carbon (IC). In addition, it had 1.10 mgL^{-1} and 1.97 mgL^{-1} of sulfate and nitrate, respectively. The river water sample was spiked with EE2 (10.0 mgL^{-1}). The removal efficiency of MPTS@BN and APTES@BN in the removal of EE2 was obtained at different pH values and shown in Fig. 9. Results indicated that the removal efficiency of EE2 using these nanocomposites in real water samples was not substantially affected compared to the treatment conducted in deionized water. Hence, the composite materials (MPTS@BN and APTES@BN) show high selectivity and applicability for attenuation of EE2 in real water samples. Therefore, materials show potential in its possible implications in the real treated waste water treatment at least for the elimination of EE2.

CONCLUSION

Bentonite is grafted with two organosilanes, i.e., 3-mercaptopropyletrimethoxy silane/or 3-aminopropyletriethoxy silane, as to obtain the MPTS@BN and APTES@BN nanocomposites. The IR studies confirmed the grafting of silanes with the bentonite network. The surface morphological studies indicated that the porous structure of bentonite becomes highly dense once silane is grafted. Further, BET specific surface area was found to be 41.11, 4.68 and 12.52 m^2g^{-1}, respectively, for the BN, MPTS@BN and APTES@BN. High percentage elimination of 17α-ethinylestradiol (EE2) was not significantly affected with increase of pH (4-10) and sorptive concentration (1.0 to 10.0 mgL^{-1}) using MPTS@BN and APTES@BN. The parametric studies indicated that the hydrophobic interaction is the driving force in the uptake of EE2 by these two nanocomposites employed. A fast uptake of EE2 attained apparent equilibrium within 120 min of contact. Moreover, the sorption data was followed by the pseudo-second-order kinetics, and the Langmuir monolayer capacity for EE2 is 8.10 and 4.28 mgg^{-1}, respectively, for MPTS@BN and APTES@BN. Increasing the background electrolytes (NaCl) by 1,000 times or presence of several co-ions could not affect the uptake of EE2 by the nanocomposites, implying the selectivity and suitability of materials towards EE2. Furthermore, a high loading capacity of EE2 was achieved using varied loadings of nanocomposites in a column. The real implication of study showed that the removal of EE2 is not affected in the river water sample. Therefore, the novel nanocomposites are useful alternative materials that are promising in remediation of water contaminated with EE2 or even for advanced treatment of treated waste water contaminated with low concentration of micro-pollutants.

SUPPORTING INFORMATION

Additional information as noted in the text. This information is available via the Internet at http://www.springer.com/chemistry/journal/11814.

REFERENCES

1. K. Kosek, A. Luczkiewicz, S. Fudala-Książek, K. Jankowska, M. Szopińska, O. Svahn, J. Tränckner, A. Kaiser, V. Langas and E. Björklund, *Environ. Sci. Policy*, **112**, 213 (2020).
2. M. Lei, L. Zhang, J. Lei, L. Zong, J. Li, Z. Wu and Z. Wang, *BioMed. Res. Int.*, **2015**, 1 (2015).
3. M. Gavrilescu, K. Demnerová, J. Aamand, S. Agathos and F. Fava, *New Biotechnol.*, **32**, 147 (2015).
4. C. P. Silva, M. Otero and V. Esteves, *Environ. Pollut.*, **165**, 38 (2012).
5. A. Bennasroune, L. Rojas, L. Foucaud, S. Goulaouic, P. Laval-Gilly, M. Fickova, N. Couleau, C. Durandet, S. Henry and J. Falla, *Int. J. Immunopathol. Pharmacol.*, **25** , 365 (2012).
6. S. Tian, Y. Liu, S. Liu, G. Zeng, L. Jiang, X. Tan, X. Huang, Z. Yin, N. Liuab and J. Liab, *RSC Adv.*, **8**, 4273 (2018).
7. S. Larcher, G. Delbès, B. Robaire and V. Yargeau, *Environ. Int.*, **39**, 66 (2012).
8. J. Han, W. Qiu, Z. Cao, J. Hu and W. Gao, *Water Res.*, **47**, 2273 (2013).
9. H. M. K. Essandoh, C. Tizaoui and M. H. A. Mohamed, *Sep. Sci. Technol.*, **47**, 777 (2012).
10. H. G. Oliveira, L. H. Ferreira, R. Bertazzoli and C. Longo, *Water Res.*, **72**, 305 (2015).
11. B. Pauwels, K. Wille, H. Noppe, H. De Brabander, T. Van de Wiele, W. Verstraete and N. Boon, *Biodegradation*, **19**, 683 (2008).
12. M. Cargouët, D. Perdiz, A. Mouatassim-Souali, S. Tamisier-Karolak and Y. Levi, *Sci. Total Environ.*, **324**, 55 (2004).
13. S. K. Atkinson, V. L. Marlatt, L. E. Kimpe, D. R. S. Lean, V. L. Trudeau and J. M. Blais, *Sci. Total Environ.*, **430**, 119 (2012).
14. S. De Assis, A. Warri, M. I. Cruz, O. Laja, Y. Tian, B. Zhang, Y. Wang, T. H.-M. Huang and L. Hilakivi-Clarke, *Nat. Commun.*, **3**, 1 (2012).
15. L. N. Vandenberg, T. Colborn, T. B. Hayes, J. J. Heindel, D. R. Jacobs Jr., D.-H. Lee, J. P. Myers, T. Shioda, A. M. Soto and F. S. vom Saal, *Reprod. Toxicol.*, **38**, 1 (2013).
16. O. T. Komesli, M. Muz, M. S. Ak, S. Bakırdere and C. F. Gokcay, *Chem. Eng. J.*, **277**, 202 (2015).
17. M. L. Scala-Benuzzi, E. A. Takara, M. Alderete, G. J. A. A. Soler-Illia, R. J. Schneider, J. Raba and G. A. Messina, *Microchem. J.*, **141**, 287 (2018).
18. M. D. Wit, D. Keil, K. van der Ven, S. Vandamme, E. Witters and W. D. Coen, *Gen. Comp. Endocrinol.*, **167**, 190 (2010).
19. Y. Feng, Z. Zhang, P. Gao, H. Su, Y. Yu and N. Ren, *J. Hazard.*

Mater., **175**, 970 (2010).
20. K. A. Kidd, P. J. Blanchfield, K. H. Mills, V. P. Palace, R. E. Evans, J. M. Lazorchak and R. W. Flick, *Proc. Natl. Acad. Sci.*, **104**, 8897 (2007).
21. P. Gao, Z. Liang, Z. Zhao, W. Wang, C. Yang, B. Hu and F. Cui, *Chemosphere*, **234**, 438 (2019).
22. F. P. Chaves, G. Gomes, A. Della-Flora, A. Dallegrave, C. Sirtori, E. M. Saggioro and D. M. Bila, *Sci. Total Environ.*, **746,** 141041 (2020).
23. S. Wang, L. Li, S. Yu, B. Dong, N. Gao and X. Wang, *Chem. Eng. J.*, **406**, 126722 (2020).
24. R. M. Castellanos, J. P. Bassin, D. M. Bila and M. Dezotti, *Environ. Pollut.*, **274**, 116551 (2021).
25. I. Anastopoulos, A. Mittal, M. Usman, J. Mittal, G. Yu, A. Núñez-Delgado and M. Kornaros, *J. Mol. Liq.*, **269**, 855 (2018).
26. H. Anjum, K. Johari, N. Gnanasundaram, M. Ganesapillai, A. Arunagiri, I. Regupathi and M. Thanabalan, *J. Mol. Liq.*, **277**, 1005 (2019).
27. N. Burham and M. Sayed, *Minerals*, **6**, 129 (2016).
28. S. Zafar, M. I. Khan, M. H. Lashari, M. Khraisheh, F. Almomani, M. L. Mirza and N. Khalid, *Emergent Mater.*, **3**, 857 (2020).
29. T. N. Soeiro, E. D. De Freitas, G. S. Maia, A. B. Santos, M. G. A. Vieira and R. Guirardello, *Chem. Eng. Trans.*, **57**, 619 (2017).
30. G. Z. Kyzas, J. Fu, N. K. Lazaridis, D. N. Bikiaris and K. A. Matis, *J. Mol. Liq.*, **209**, 87 (2015).
31. J. He, J. Guo, Q. Zhou, J. Yang, F. Fang and Y. Huang, *Chemosphere*, **216**, 59 (2019).
32. A. E. Burgos, T. A. Ribeiro-Santos and R. M. Lago, *Water Sci. Technol. J. Int. Assoc. Water Pollut. Res.*, **74**, 663 (2016).
33. G. K. Dinesh and S. Chakma. *J. Taiwan Inst. Chem. Eng.*, **100**, 95 (2019).
34. R. Chauhan, G. K. Dinesh, B. Alawa and S. Chakma, *Chemosphere*, **277**, 130324 (2021).
35. G. K. Dinesh and S. Chakma, *Ultrason. Sonochem.*, **50**, 311 (2019).
36. V. V. Kumar, D. Avisar, V. Lakshmi Prasanna, Y. Betzalel and H. Mamane, *J. Hazard. Mater.*, **398**, 122880 (2020).
37. L. P. Vaddadi, D. Avisar, V. K. Vadivel, O. Menashe, E. Kurzbaum, V. Cohen-Yaniv and H. Mamane, *Materials*, **13**, 83 (2019).
38. L. Mita, M. Forte, A. Rossi, C. Adamo, S. Rossi, D. G. Mita, M. Guida, M. Portaccio, T. Godievargova and I. Yavour, *Ann. Environ. Sci. Toxicol.*, **2**, 048 (2017).
39. J. Han, W. Qiu, S. Meng and W. Gao, *Water Res.*, **46**, 5715 (2012).
40. A. K. Kumar and S. V. Mohan, *Desalination*, **276**, 66 (2011).
41. J. Rudder, T. V. Wiele, W. Dhooge, F. Comhaire and W. Verstraete, *Water Res.*, **38**, 184 (2004).
42. C. Díaz-Quiroz, L. González, M. S. Álvarez, J. F. Hernandez-Chavez, A. Rodriguez, F. J. Delve and G. Ulloa-Mercado, *Sep. Purif. Technol.*, **250**, 117068 (2020).
43. M. Belhadri, M. Sassi and A. Benguedach, *J. Water Chem. Technol.*, **41**, 357 (2019).
44. N. G. Turan and O. Ozgonenel, *Sci. World J.*, **2013**, 342628 (2013).
45. T. K. Sen and D. Gomez, *Desalination*, **267**, 286 (2011).
46. J. Guo, S. Chen, L. Liu, B. Li, P. Yang, L. Zhang and Y. Feng, *J. Colloid Interface Sci.*, **382**, 61 (2012).
47. D. Tiwari and S. M. Lee, *Chem. Eng. J.*, **204-206**, 23 (2012).
48. S. M. Lee, Lalhmunsiama, Thanhmingliana and D. Tiwari, *Chem. Eng. J.*, **270**, 496 (2015).
49. Lalhmunsiama, S. M. Lee and D. Tiwari, *Chem. Eng. J.*, **225**, 128 (2013).
50. Lalchhingpuii, D. Tiwari, Lalhmunsiama and S. M. Lee, *Chem. Eng. J.*, **328**, 434 (2017).
51. V. Marjanović, S. Lazarević, I. Janković-Častvan, B. Potkonjak, Đ. Janaćković and R. Petrović, *Chem. Eng. J.*, **166**, 198 (2011).
52. T. Şahan, F. Erol and Ş. Yılmaz, *Microchem. J.*, **138**, 360 (2018).
53. Ş. Yılmaz, T. Şahan and A. Karabakan, , *Korean J. Chem. Eng.*, **34**, 2225 (2017).
54. X. Liang, Y. Xu, G. Sun, L. Wang, Y. Sun, Y. Sun and X. Qin, *Chem. Eng. J.*, **174**, 436 (2011).
55. W. Carvalho, C. Vignado and J. Fontana, *J. Hazard. Mater.*, **153**, 1240 (2008).
56. T. C. Perrotti, N. S. Freitas, M. Alzamora, D. R. Sánchez and N. M. Carvalho, *J. Environ. Chem. Eng.*, **7**, 103237 (2019).
57. M. Asgari, A. Abouelmagd and U. Sundararaj, *Appl. Clay Sci.*, **146**, 439 (2017).
58. F. Piscitelli, P. Posocco, R. Toth, M. Fermeglia, S. Pricl, G. Mensitieri and M. Lavorgna, *J. Colloid Interface Sci.*, **351**, 108 (2010).
59. Z. Qin, P. Yuan, S. Yang, D. Liu, H. He and J. Zhu, *Appl. Clay Sci.*, **99**, 229 (2014).
60. B. Paul, W. N. Martens and R. L. Frost, *Appl. Surf. Sci.*, **257**, 5552 (2011).
61. A. Walcarius, M. Etienne and J. Bessière, *Chem. Mater.*, **14**, 2757 (2002).
62. A. Xue, S. Zhou, Y. Zhao, X. Lu and P. Han, *J. Hazard. Mater.*, **194**, 7 (2011).
63. H. Cui, Y. Qian, Q. Li, Z. Wei and J. Zhai, *Appl. Clay Sci.*, **72**, 84 (2013).
64. A. Košak, A. Lobnik and M. Bauman, *Int. J. Appl. Ceram. Technol.*, **12**, 461 (2015).
65. S. B. Y. Abeywardena, S. Perera, K. M. Nalin de Silva and N. P. Tissera, *Int. Nano Lett.*, **7**, 237 (2017).
66. T. X. Bui, S.-Y. Kang, S.-H. Lee and H. Choi, *J. Hazard. Mater.*, **193**, 156 (2011).
67. L. A. Al-Khateeb, A. Y. Obaid, N. A. Asiri and M. Abdel Salam, *J. Ind. Eng. Chem.*, **20**, 916 (2014).
68. Lalhmunsiama, Lalchhingpuii, B. P. Nautiyal, D. Tiwari, S. I. Choi, S. H. Kong and S. M. Lee, *J. Colloid Interface Sci.*, **467**, 203 (2016).
69. Y. Zhang and J. L. Zhou, *Water Res.*, **39**, 3991 (2005).
70. Lalhmunsiama, S.-M. Lee, Lalchhingpuii and D. Tiwari, *J. Environ. Chem. Eng.*, **4**, 1537 (2016).
71. Z. Hasan, E.-J. Choi and S. H. Jhung, *Chem. Eng. J.*, **219**, 537 (2013).
72. C. B. Vidal, J. T. Oliveira, G. S. C. Raulino, D. de Q. Melo, G. P. Pessoa, A. B. dos Santos and R. F. do Nascimento, *XX Congresso Brasileiro de Engenharia Quima.*, **1**, 2 (2014).
73. S. M. Lee, D. Tiwari and S. K. Prasad, *RSC Adv.*, **5**, 46834 (2015).
74. A. O. Ifelebuegu, J. E. Ukpebor, C. C. Obidiegwu and B. C. Kwofi, *Glob. J. Environ. Sci. Manag.*, **1**, 205 (2015).
75. T. Thanhmingliana, S. M. Lee, D. Tiwari and S. K. Prasad, *RSC Adv.*, **5**, 46834 (2015).
76. L. Joseph, Q. Zaib, I. A. Khan, N. D. Berge, Y.-G. Park, N. B. Saleh and Y. Yoon, *Water Res.*, **45**, 4056 (2011).
77. P. Gao, C. Yang, Z. Liang, W. Wang, Z. Zhao, B. Hu and F. Cui, *Chemosphere*, **214**, 361 (2019).

Supporting Information

17α-Ethinylestradiol elimination using synthesized and dense nanocomposite materials: Mechanism and real matrix treatment

Ralte Malsawmdawngzela and Diwakar Tiwari[†]

Department of Chemistry, Mizoram University, Aizawl-796004, India
(*Received 14 July 2021 • Revised 12 September 2021 • Accepted 14 September 2021*)

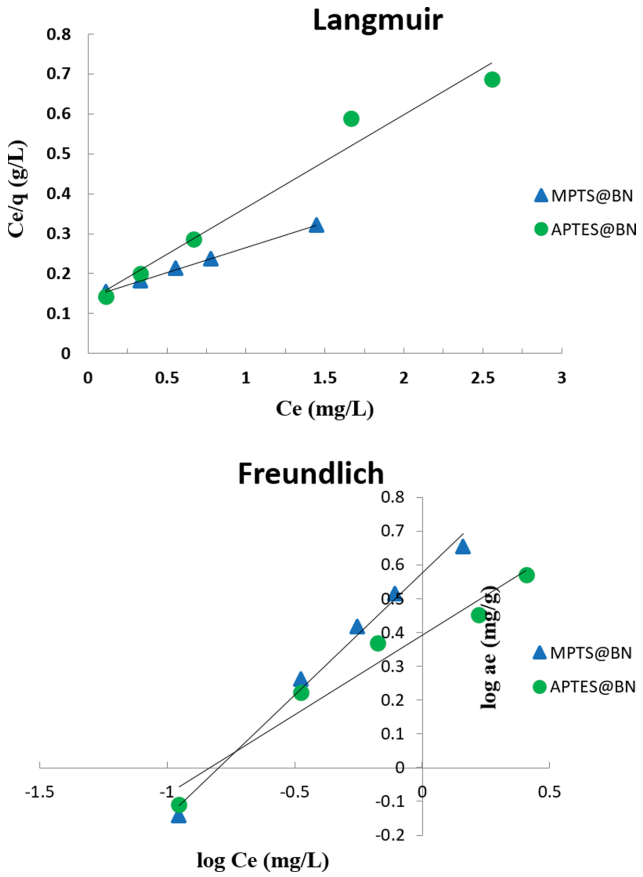

Fig. S1. Fitting of (a) Langmuir (b) Freundlich isotherm in the sorption of EE2 by MPTS@BN and APTES@BN materials.

Table S1. Different parameteric resulst obtained for real water (collected from Kawnpui river water at Kolasib District, Mizoram, India) sample

Elements studied (AAS Measurements)	(mgg^{-1})
Fe	0.0214
Zn	0.0021
Mn	0.0701
Ca	0.51
Pb	0.0001
Cu	0.0001
TOC analysis	mgL^{-1}
IC	1.45
NPOC	8.95
Anions studied	mgL^{-1}
Sulphate	1.101
Phosphate	0.076
Fluoride	0
Nitrate	1.975